

Temperature, Oxygen, and Salt-Sensing Neurons in *C. elegans* Are Carbon Dioxide Sensors that Control Avoidance Behavior

Andrew Jonathan Bretscher,¹ Eiji Kodama-Namba,¹ Karl Emanuel Busch,¹ Robin Joseph Murphy,¹ Zoltan Soltesz,¹ Patrick Laurent,¹ and Mario de Bono^{1,*}

¹MRC Laboratory of Molecular Biology, Hills Road, Cambridge CB2 0QH, UK

*Correspondence: debono@mrc-lmb.cam.ac.uk

DOI 10.1016/j.neuron.2011.02.023

Open access under [CC BY](https://creativecommons.org/licenses/by/4.0/) license.

SUMMARY

Homeostatic control of body fluid CO₂ is essential in animals but is poorly understood. *C. elegans* relies on diffusion for gas exchange and avoids environments with elevated CO₂. We show that *C. elegans* temperature, O₂, and salt-sensing neurons are also CO₂ sensors mediating CO₂ avoidance. AFD thermosensors respond to increasing CO₂ by a fall and then rise in Ca²⁺ and show a Ca²⁺ spike when CO₂ decreases. BAG O₂ sensors and ASE salt sensors are both activated by CO₂ and remain tonically active while high CO₂ persists. CO₂-evoked Ca²⁺ responses in AFD and BAG neurons require cGMP-gated ion channels. Atypical soluble guanylate cyclases mediating O₂ responses also contribute to BAG CO₂ responses. AFD and BAG neurons together stimulate turning when CO₂ rises and inhibit turning when CO₂ falls. Our results show that *C. elegans* senses CO₂ using functionally diverse sensory neurons acting homeostatically to minimize exposure to elevated CO₂.

INTRODUCTION

As the major by-product of oxidative metabolism, CO₂ is ubiquitous in nature. Although CO₂ comprises only ~0.038% of Earth's atmosphere, it can accumulate to higher levels in environments with high respiration rates (Lahiri and Forster, 2003). Organisms have evolved CO₂-sensing mechanisms to monitor both external and internal CO₂ concentrations, but how these systems function to control physiology and behavior remain poorly understood.

Mice can smell environmental CO₂ concentrations as low as 0.066% CO₂ using specialized olfactory neurons that express carbonic anhydrase II (Hu et al., 2007). Carbonic anhydrases catalyze hydration of CO₂ to generate H⁺ and HCO₃⁻. HCO₃⁻ is thought to stimulate the mouse olfactory neurons by activating a guanylate cyclase, GC-D (Hu et al., 2007; Sun et al., 2009). In humans the GC-D homolog is a pseudogene, and we cannot smell CO₂ (Young et al., 2007). However, we can taste CO₂ in carbonated solutions via sour-sensing cells on our tongues (Chandrasekar et al., 2009). In rodents, CO₂ levels of 10% or more elicit

an innate fear response in which animals freeze and avoid open spaces (Ziemann et al., 2009). This response requires activation of the acid-sensing ion channel ASIC-1A in cells of the amygdala (Ziemann et al., 2009). High concentrations of inhaled CO₂ also modulate wakefulness by stimulating midbrain neurons (Williams et al., 2007; Richerson, 2004; Buchanan and Richerson, 2010).

Insects also sense and respond to environmental CO₂. *Drosophila* adults and larvae avoid CO₂ levels as low as 0.1% (Suh et al., 2004; Faucher et al., 2006). Like the CO₂-evoked fear behavior in mice, *Drosophila* CO₂ avoidance is innate (Suh et al., 2004) and may be part of an alarm response: stressed flies release 3- to 4-fold more CO₂ than unstressed flies (Suh et al., 2004). *Drosophila* senses gaseous CO₂ using two olfactory receptors, *Gr21a* and *Gr63a*, which are expressed in antennal sensory neurons (Jones et al., 2007; Kwon et al., 2007). Like other insect olfactory receptors, these do not have homologs in vertebrates or worms (Vosshall and Stocker, 2007). Artificial activation of the *Gr21a/Gr63a*-expressing neurons elicits an avoidance response (Suh et al., 2007). Whether the *Gr21a/Gr63a* receptor binds molecular CO₂ or a CO₂ derivative is not known. Interestingly, some food-associated odorants inhibit *Gr21a/Gr63a* CO₂ receptor function, and the presence of food reduces CO₂ avoidance (Turner and Ray, 2009). Although *Drosophila* avoids gaseous CO₂, it is attracted to carbonated substrates, a response mediated by HCO₃⁻-sensitive neurons in the proboscis (Fischler et al., 2007).

Besides monitoring external CO₂, many animals also monitor internal CO₂. Internal CO₂ levels are regulated by respiratory gas exchange (Lahiri and Forster, 2003; Feldman et al., 2003; Bustami et al., 2002), but when left unregulated can lead to toxic changes in body fluid pH and death (Richerson, 2004). Mammalian respiratory CO₂ chemoreception occurs in the brain and carotid bodies (Lahiri and Forster, 2003). The molecular mechanisms are unclear, but CO₂-sensitive cells express carbonic anhydrases (Coates et al., 1998; Cammer and Brion, 2000), and changes in extracellular or intracellular pH modulate signaling via H⁺-sensitive ion channels (Lahiri and Forster, 2003; Richerson et al., 2005; Buckler et al., 2000; Feldman et al., 2003; Richerson, 2004; Jiang et al., 2005). Insects achieve respiratory gas exchange by opening and closing spiracles, but the control mechanisms involved are not known (Hetz and Bradley, 2005; Lehmann and Heymann, 2005).

Many small animals, including the nematode *C. elegans*, lack a specialized respiratory system and use diffusion for gas

exchange. As in other animals, high CO₂ levels are toxic (Sharabi et al., 2009). *C. elegans* appears to control internal CO₂ by avoiding environments where this gas exceeds ~0.5%. Avoidance requires cGMP-gated ion channels containing the TAX-2 and TAX-4 subunits (Bretscher et al., 2008; Hallem and Sternberg, 2008). Also implicated are the BAG sensory neurons, required for acute avoidance of a high CO₂ and low O₂ mixture (Hallem and Sternberg, 2008). Recent work indicates that the BAG neurons are transiently activated when ambient O₂ levels fall below 10% (Zimmer et al., 2009).

Here, we show that the *C. elegans* head sensory neurons AFD, BAG, and ASE are primary CO₂ sensors. AFD, BAG, and ASE were previously only known to detect changes in temperature, O₂, and salt ion levels, respectively. Using Ca²⁺ imaging, we describe the CO₂ responses of these neurons, which include ON, OFF, and perduring responses. We show that some, but not all, of the Ca²⁺ responses to CO₂ depend on a cGMP-gated ion channel. Finally, we dissect how the *C. elegans* CO₂ sensory system regulates CO₂-evoked behavior. We find that the contribution of different sensors to behavior varies widely, depending on both context and stimulus dynamics.

RESULTS

Multiple Sensory Neurons Mediate *C. elegans* Avoidance of CO₂

When placed in a 5%-0% CO₂ gradient, *C. elegans* migrate away from high CO₂ (Figures 1A and 1B) (Bretscher et al., 2008). We used this assay to identify potential CO₂-sensing neurons. Mutants defective in either the TAX-4 α or TAX-2 β cGMP-gated ion channel subunits show reduced CO₂ avoidance, both in the presence and absence of *E. coli* food (Figure 1C) (Bretscher et al., 2008; Hallem and Sternberg, 2008). The defects of *tax-2*; *tax-4* double mutants recapitulated those of single mutants (Figure 1C), consistent with α and β subunits functioning together. *tax-2* and *tax-4* are coexpressed in 14 of 40 *C. elegans* sensory neuron classes (White et al., 1986; Komatsu et al., 1996; Coburn and Bargmann, 1996), implicating a subset of these neurons in CO₂ sensing. A *tax-2* promoter mutation, *tax-2(p694)*, also disrupted CO₂ avoidance (Figure 1C). Previous work reported that this allele deletes exon 1 and ~1.6 kb of *tax-2* upstream sequences (Coburn and Bargmann, 1996). However, our sequencing data suggest that it removes only 365 bp in this interval (details in Supplemental Experimental Procedures available online). *tax-2(p694)* mutants have deficits in behaviors mediated by the AFD, BAG, ASE, AQR, PQR, and URX neurons but appear wild-type for responses mediated by other *tax-2* expressing neurons (Dusenbery et al., 1975; Hedgecock and Russell, 1975; Coburn and Bargmann, 1996; Coates and de Bono, 2002). Selectively expressing *tax-2* cDNA in AFD, BAG, ASE, AQR, PQR, and URX in *tax-2(p694)* mutants restored CO₂ avoidance to the same extent as a full-length *tax-2* genomic fragment (Figures 1C and 1D). We next attempted to rescue the *tax-2(p694)* defect by expressing *tax-2* cDNA from neuron-specific promoters, confirming appropriate expression by polycistronic constructs that coexpress *tax-2* and *gfp* (Coates and de Bono, 2002). Expressing *tax-2* cDNA in the AFD thermosensory neurons strongly rescued CO₂ avoidance, both on and off food

(Figure 1D). In contrast, restoring *tax-2* to the BAG O₂-sensing neurons rescued CO₂ avoidance on food, as shown previously (Hallem and Sternberg, 2008), but not off food. Expressing *tax-2* cDNA in the ASE taste neurons or in the AQR, PQR, and URX O₂-sensing neurons also partially rescued CO₂ avoidance, both on food and off food (Figure 1D). These data implicate functionally diverse sensory neurons in CO₂ avoidance.

The AFD Thermosensory Neurons Sense CO₂

The AFD neurons are transiently activated when temperatures exceed cultivation levels (Kimura et al., 2004; Clark et al., 2006). To test whether AFD also responds to CO₂, we monitored AFD intracellular Ca²⁺ levels during CO₂ exposure using the ratiometric Ca²⁺ sensor cameleon YC3.60, expressed in AFD under control of the *gcy-8* promoter (Yu et al., 1997). Animals expressing the Ca²⁺ sensor retained wild-type CO₂ responses (Figure S1A; see Experimental Procedures). To deliver CO₂ stimuli, we used a Y-shaped microfluidic chamber that enables the gas phase over an immobilized animal to be switched in less than 3 s (Persson et al., 2009). In all experiments, O₂ was maintained at 21%, with nitrogen (N₂) completing the balance. AFD Left and AFD Right neurons responded equally to CO₂ (Figure 2A; data not shown). On CO₂ exposure the AFD neurons exhibited a fall in intracellular Ca²⁺ that slowly reversed to rise above baseline levels (“CO₂-ON” response) within 2 min of CO₂ coming on (Figures 2A and 2C). Thus, the AFD CO₂-ON response has two components to it, an “ON-minimum” and an “ON-maximum.” Strikingly, AFD also responded to removal of CO₂ with a fast Ca²⁺ spike that peaked within 10 s (“CO₂-OFF” response, Figures 2A and 2D). The OFF-maximum was the largest feature of the AFD Ca²⁺ pattern, being on average 3- to 4-fold greater than the ON-maximum (Figure 2B). All three components of the AFD CO₂ response were concentration dependent (Figure 2B). To exclude the possibility that the observed activity could be due to AFD temperature sensing, we exposed animals to 0%-0%-0% CO₂ mock switches. Under these conditions AFD gave no responses (first 9 min, Figure 2E).

We next examined whether repeated stimulation altered AFD Ca²⁺ responses. Some *C. elegans* sensory neurons, such as the ALM anterior touch neurons, habituate upon repeated stimulation (Kindt et al., 2007). The AFD OFF response remained undiminished upon repeated exposure to 3% CO₂ (Figures 2E, 2F, and S1B). We also asked whether prolonged CO₂ exposure affects AFD responses. After a 9 min exposure to 3% CO₂, the ON-maximum had decayed to baseline levels, whereas the OFF-maximum was unaltered (Figure 2G).

CO₂-evoked activity in AFD could be due to synaptic input to AFD. To test this, we imaged CO₂ responses in *unc-13* mutants, which have severe defects in synaptic release (Richmond et al., 1999). The AFD CO₂ responses of *unc-13* animals were indistinguishable from wild-type (Figures 2H and S1C). These data suggest that, as well as being a thermosensory neuron (Mori and Ohshima, 1995; Kimura et al., 2004; Clark et al., 2007), AFD is a CO₂ sensor with both ON and OFF responses. The sensory endings of AFD have many finger-like projections, potentially providing a large surface for CO₂ and temperature reception (Ward et al., 1975).

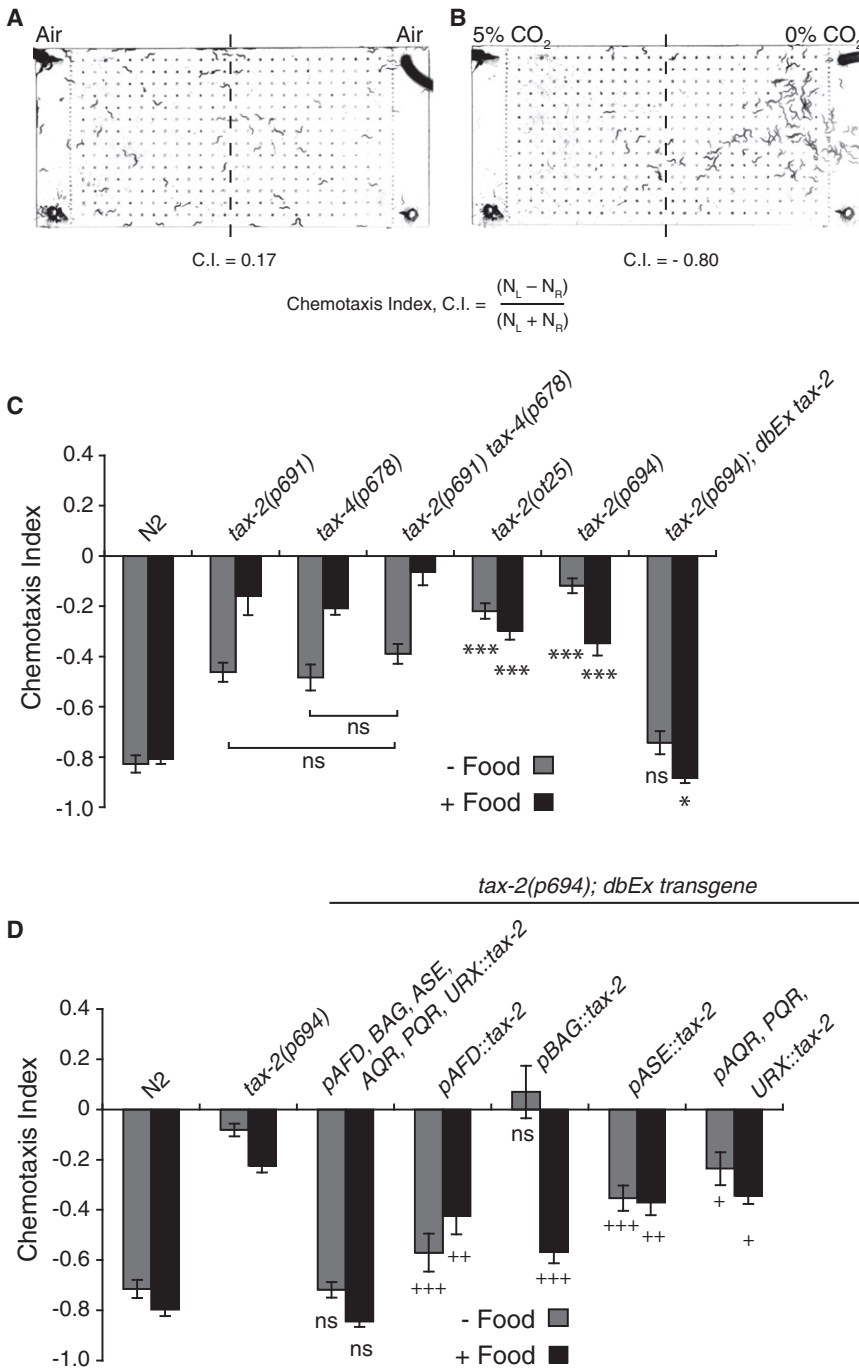


Figure 1. The cGMP-Gated Ion Channel Subunit TAX-2 Acts in Multiple Neurons to Promote CO₂ Avoidance

(A and B) Wild-type *C. elegans* distribute uniformly in air (A) but avoid 5% CO₂ (B) over 10 min. N_L and N_R, the number of animals in the left and right halves of the chamber, respectively.

(C) Mutations in the cGMP-gated ion channel subunits *tax-2* and *tax-4* disrupt avoidance of 5% CO₂ both on and off food. The null allele *tax-2(ot25)* and promoter deletion allele *tax-2(p694)* almost completely abolish CO₂ avoidance. A transgene containing *tax-2* genomic DNA restores CO₂ avoidance to *tax-2(p694)* mutants. In this and all subsequent figures, unless otherwise stated: a 5%-0% CO₂ gradient was used; data points represent an average of nine assays; error bars indicate standard error of the mean (SEM); ns, not significantly different; *** or +++ indicates p < 0.001; ** or ++ indicates p < 0.01; * or + indicates p < 0.05; and significance comparisons were made using the two-tailed Student's t test.

(D) Expressing full-length *tax-2* cDNA in the AFD, BAG, ASE, and AQR, PQR, and URX neurons rescues CO₂ avoidance in *tax-2(p694)* mutants. Expressing *tax-2* cDNA from the neuron-specific promoters *pgcy-8* (AFD), *pflp-17* (BAG), and an ASE-specific *pflp-6* fragment or *pgcy-32* (AQR, PQR, URX) gives varying degrees of rescue. Significance comparison of the transgenic line expressing *tax-2* in all six neurons is with N2. For all other genotypes, significance markers indicate comparison with *tax-2(p694)*.

support the idea that AFD CO₂ and temperature-sensing pathways are at least partly distinct.

The BAG O₂ Sensory Neurons Sense CO₂

Recent work has shown that the BAG neurons are transiently activated when O₂ levels drop below 10% (Zimmer et al., 2009). Hallem and Sternberg (2008) showed that feeding animals lacking the BAG neurons have reduced avoidance of a 10% CO₂/10% O₂ mixture. We have previously shown that O₂ responses can modulate CO₂ avoidance (Bretscher et al., 2008). These data suggest that either BAG responds exclusively to O₂

but modulates neural circuits mediating CO₂ responses or that BAG is a primary sensor of both O₂ and CO₂.

AFD only responds to a temperature rise above the cultivation temperature (Kimura et al., 2004; Clark et al., 2006). If AFD temperature and CO₂-sensing are distinct, AFD might be expected to respond to CO₂ at temperatures below the cultivation temperature. To test this, we built a temperature-controlled stage (see Supplemental Experimental Procedures). In animals grown at 22°C, AFD responded to CO₂ both at 15°C and at 22°C (Figures S1E and S1F). The shape of the response was similar at the two temperatures but smaller at 15°C than at 22°C. These data

but modulates neural circuits mediating CO₂ responses or that BAG is a primary sensor of both O₂ and CO₂.

To test BAG neuron CO₂ sensitivity, we created animals expressing transgene YC3.60 in BAG from a *pflp-17::YC3.60* transgene and imaged Ca²⁺ levels. The BAGL and BAGR neurons were exquisitely sensitive to a rise in CO₂ (Figures 3A–3C). Cameleon reported a rise in Ca²⁺ that peaked after ~30 s and then decayed (Figures 3A and 3B). The excitability threshold of BAG was below 0.25% CO₂. A plot of mean fluorescence ratio

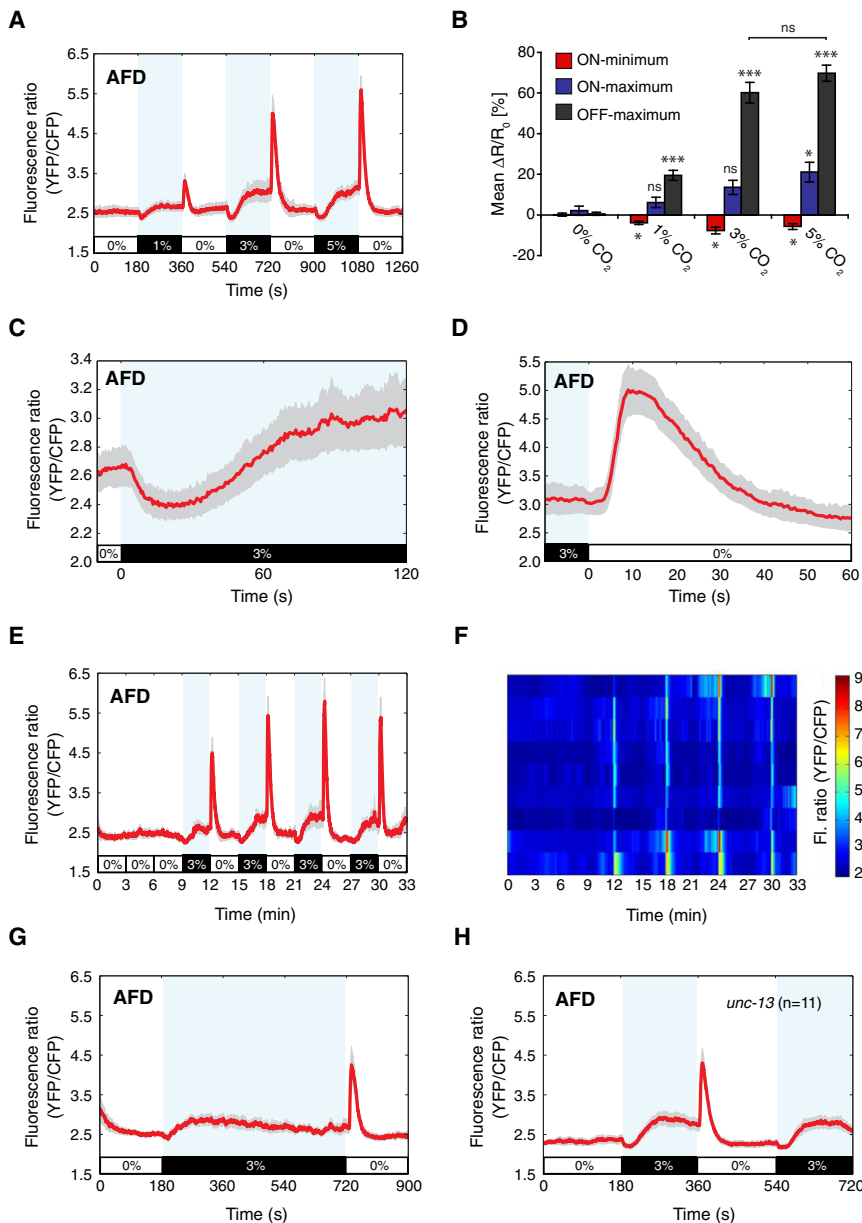


Figure 2. The AFD Thermosensory Neurons Sense CO₂

(A) Mean fluorescence ratio (YFP/CFP) of AFD neurons expressing cameleon YC3.60 across a 0%-1%-0%-3%-0%-5%-0% CO₂ stimulus. In this and all subsequent figures, blue shading indicates presence of CO₂, and gray shading indicates the SEM (n = 26 traces).

(B) Mean ratio change, ΔR , expressed as a percentage of the initial fluorescence ratio, R_0 , for the AFD ON and OFF responses for mock, 1%, 3%, and 5% CO₂ concentrations. $\Delta R = R_f - R_0$, where R_f is the fluorescence ratio after gas shift. Time intervals for calculation of R_f and corresponding intervals for R_0 , were chosen according to peaks in ratio change. For ON-minima, a 20 s time interval was used, for ON-maxima a 30 s interval, and for OFF-maxima an 8 s interval. Data for 1%, 3%, and 5% steps from (A); data for mock step from (E). Details for 1%, 3%, and 5% steps: ON-minima (150–170 s and 190–210 s, 510–530 s, and 550–570 s, 870–890 s and 910–930 s, used for R_0 and R_f , respectively); ON-maxima (150–180 s and 330–360 s, 510–540 s, and 690–720 s, 870–900 s, and 1050–1080 s, used for R_0 and R_f , respectively); OFF-maxima (344–352 s and 368–376 s, 704–712 s and 728–736 s, 1064–1072 s and 1088–1096 s, used for R_0 and R_f , respectively). Significance markers indicate comparisons with responses to a mock 0% CO₂ gas switch. Error bars indicate SEM.

(C and D) Expanded view of mean AFD response to a 0%-3% CO₂ increase (C) and 3%-0% CO₂ decrease (D). Data from (A).

(E and F) Mean AFD response to multiple 3% CO₂ stimuli (E) and individual responses (F) plotted in a heat map (n = 9 traces).

(G) Mean AFD response to a 3% CO₂ stimulus lasting 9 min (n = 9 traces).

(H) Mean AFD response to 3% CO₂ in an *unc-13* mutant.

change against percent (%) CO₂ suggests that BAG reaches half-maximal activity at ~2.9% CO₂ (Figure 3D). Thus, BAG neurons respond to both O₂ and CO₂.

Elevated CO₂ persistently stimulates locomotory activity in feeding *C. elegans*, suggesting that some CO₂-sensing circuits can signal tonically in high CO₂ (Bretscher et al., 2008). During prolonged high CO₂ the BAG Ca²⁺ spike decayed to a plateau that persisted until CO₂ removal, at which point Ca²⁺ returned to resting levels (Figure 3E). Thus, BAG exhibits both a transient peak and a perduring Ca²⁺ plateau in response to elevated CO₂. As with AFD, we asked whether BAG neurons habituate. During five stimulus cycles of 3% CO₂, BAG showed a decrement in response amplitude after the first CO₂ stimulus, but no habituation thereafter (Figures 3F–3H).

To test if the BAG neurons are primary CO₂ sensors, we disrupted synaptic input to BAG using the *unc-13* and *unc-31* mutations. *unc-31* mutants are defective in dense-core vesicle release, but not synaptic vesicle release (Speese et al., 2007). Neither the *unc-13* nor the *unc-31* mutations disrupted BAG Ca²⁺ responses, suggesting that BAG neurons are intrinsically CO₂ sensitive (Figures 3I–3K). However, the magnitude of Ca²⁺ responses in these mutants was significantly enhanced, particularly in *unc-31* animals, suggesting that BAG activity is normally inhibited by neuromodulators.

The Asymmetric ASEL and ASER Taste Neurons Are Both Activated by CO₂

We next examined CO₂ responses in the ASE neurons that mediate chemotaxis to water-soluble cues, including salt ions such as Na⁺ and Cl⁻ (Bargmann and Horvitz, 1991; Ortiz et al., 2009). ASEL and ASER are functionally asymmetric (Hobert et al., 2002). ASEL is activated by a rise in the concentration of NaCl,

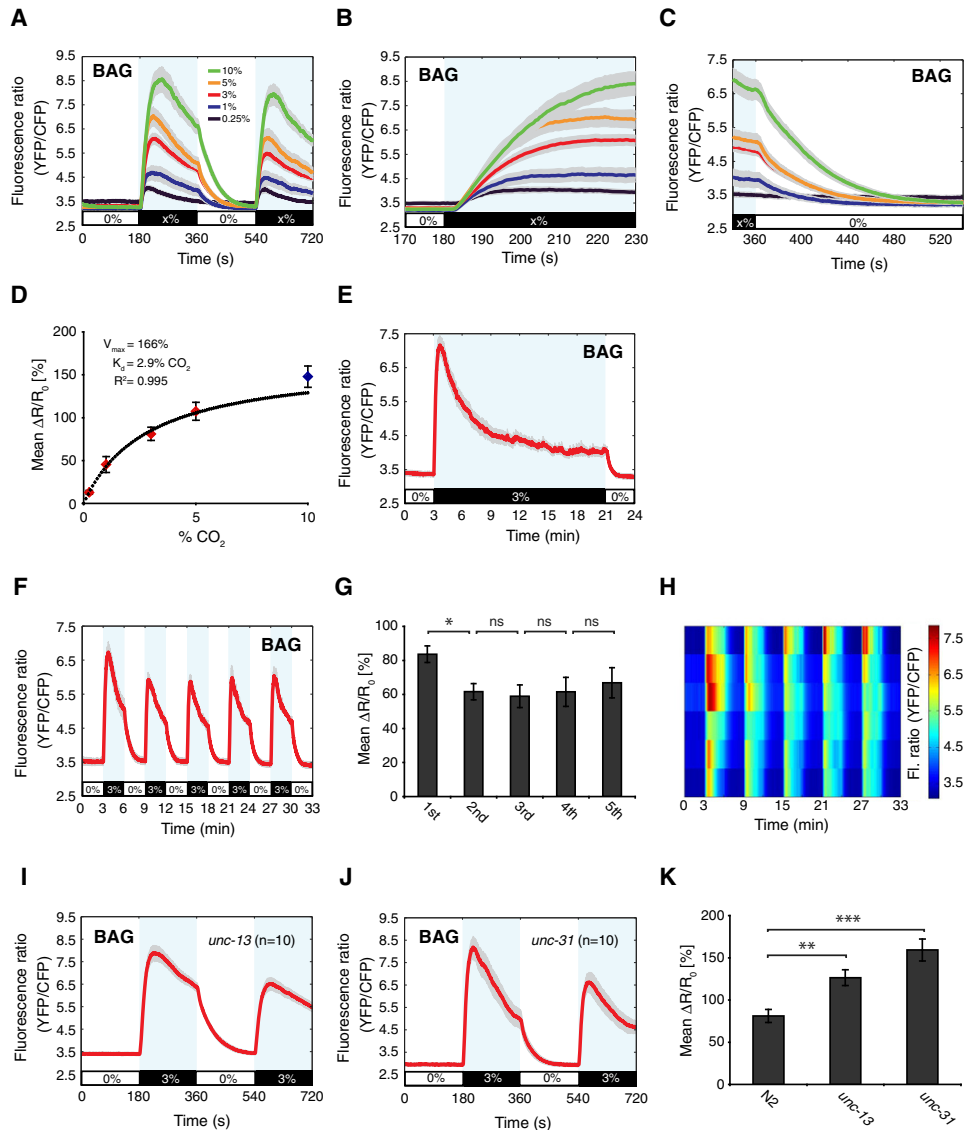


Figure 3. The BAG Neurons Are Highly Sensitive to CO₂

(A–C) The BAG neurons exhibit a large “CO₂-ON” response. Mean BAG responses to 0%-x%-0%-x% CO₂ stimuli for x = 0.25%, 1%, 3%, 5%, or 10% CO₂. Shown are the full response (A), a 60 s interval across CO₂ introduction (B), and a 180 s interval across CO₂ removal (C) (n = 10 or more traces for all concentrations).

(D) Dose-response curve for the BAG CO₂ response. The mean fluorescence ratio change, ΔR , is plotted as a percentage of the mean baseline fluorescence ratio, R_0 . $\Delta R = R_f - R_0$. R_f was calculated from the peak of the BAG Ca²⁺ response at 200–260 s and R_0 from 120–180 s. Curve fit of the standard equation for a single-site binding process (Michaelis-Menten, $y = V_{max}x/(K_d + x)$, where V_{max} and K_d are constants with units of [% mean ratio change] and % CO₂, respectively) to the red data points using least-squares regression analysis. The blue data point (10% CO₂) was omitted from the curve fit because at 10% CO₂ the BAG fluorescence ratio (YFP/CFP) falls outside of the linear dynamic range of the Ca²⁺ sensor YC3.60. Curve fit gives $K_d = 2.9\%$ CO₂, and $V_{max} = 166\%$ mean $\Delta R/R_0$, with a goodness of fit R^2 regression value of 0.995. Error bars indicate SEM.

(E) Mean BAG response to a 3% CO₂ stimulus lasting 18 min (n = 9 traces).

(F–H) BAG responses to a 0%-3%-0%-3%-0%-3%-0%-3%-0%-3%-0% CO₂ stimulus. (F) Mean fluorescence ratio (YFP/CFP), (G) mean percent (%) $\Delta R/R_0$, and individual BAG Ca²⁺ traces plotted in a heat map (H) (n = 6 traces).

(I–K) Mean BAG Ca²⁺ responses in *unc-13* mutants (I) and *unc-31* mutants (J). (K) Mean percent (%) $\Delta R/R_0$ values for (I) and (J). Asterisks indicate significance compared to wild-type.

whereas ASER is activated by a drop (Suzuki et al., 2008). For NaCl responses, activation of ASEL inhibits animals from reversing, whereas activation of ASER increases reversal likelihood (Suzuki et al., 2008).

We imaged ASEL and ASER Ca²⁺ responses to CO₂, using animals expressing the Ca²⁺ sensor YC2.12 in ASE from a *pflp-6::YC2.12* transgene (Suzuki et al., 2008). Both ASEL and ASER were activated by 1%, 3%, and 5% CO₂ (Figures

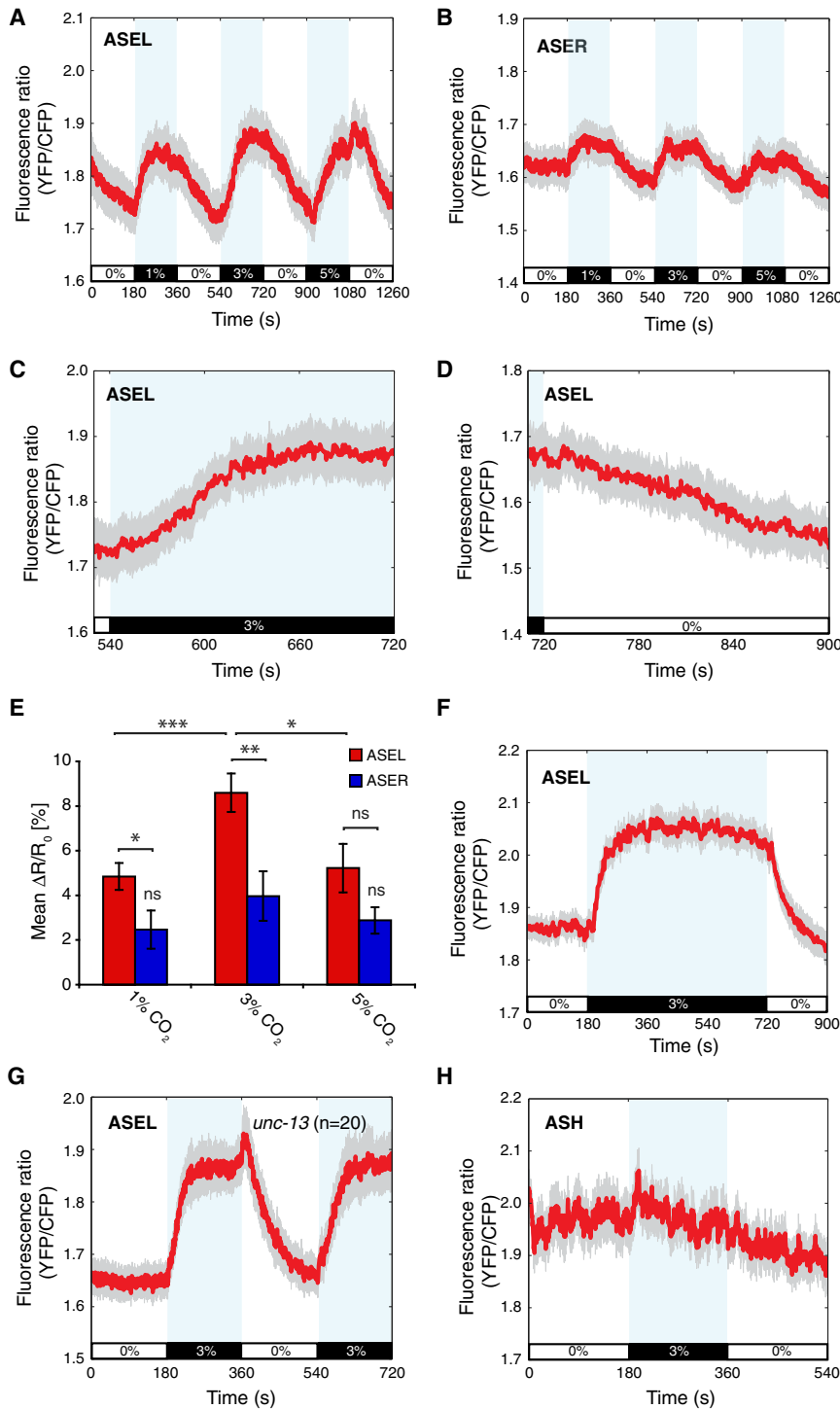


Figure 4. The ASEL and ASER Neurons Are Activated by CO₂

(A and B) Mean responses of ASEL (A) and ASER (B) to 0%-1%-0%-3%-0%-5%-0% CO₂. ASEL, n = 26 traces; ASER, n = 19 traces.

(C and D) Expanded view of mean ASEL response to a 0%-3% CO₂ increase (C) and 3%-0% CO₂ decrease (D).

(E) Mean percent (%) $\Delta R/R_0$ for ASEL and ASER for 1%, 3%, and 5% CO₂ stimuli. Baseline ratio, R_0 , was calculated from the 60 s before CO₂ exposure, and peak ratio, R_t , was calculated from the 60 s before CO₂ removal. ASER responses to 1% and 5% CO₂ are not significantly different from responses to 3% CO₂. ASEL responses to 1% and 5% CO₂ are significantly different from responses to 3% CO₂. ASEL responses are significantly different from ASER responses for 1% and 3% CO₂, but not 5% CO₂.

(F) Mean ASEL response to a 3% CO₂ stimulus lasting 9 min (n = 14 traces).

(G) Mean ASEL response to 3% CO₂ in an *unc-13* mutant.

(H) The ASH neurons are not activated by 3% CO₂ (n = 21 traces).

in *unc-13* mutants (Figures 4G and S1D). In summary, ASEL and ASER both respond to CO₂ by a slow rise in Ca²⁺ that persists while CO₂ is high and returns to baseline when CO₂ returns to baseline.

AQR, PQR, and URX O₂-Sensing Neurons Are Weakly CO₂ Responsive

We examined whether the AQR, PQR, and URX O₂-sensing neurons (Persson et al., 2009; Zimmer et al., 2009) respond to CO₂ because our *tax-2* rescue data indicated that these neurons contribute, albeit weakly, to CO₂ avoidance. Average Ca²⁺ traces indicated that unlike AFD, BAG, and ASE, none of these neurons respond reliably to CO₂ (Figures S2A–S2D). URX most consistently showed CO₂-evoked activity, and this was retained in *unc-13* mutants (Figures S2A, S2E, and S2F). AQR and PQR occasionally showed a Ca²⁺ rise associated with an increase in CO₂ but also showed apparent spontaneous activity that lay out of synchrony with the CO₂ stimulus (Figures S2B–S2D). The response of

4A–4E), although the responses of ASEL were generally ~2-fold larger than those of ASER (Figure 4E). ASEL responses to CO₂ were slow, taking around 2 min for Ca²⁺ levels to peak (Figure 4F). Sustained elevated CO₂ led to sustained increases in Ca²⁺ (Figure 4F). As for AFD and BAG, ASEL neurons appeared to be intrinsically CO₂ sensitive because Ca²⁺ responses were intact

PQR to a 0%-3%-0%-3% CO₂ stimulus was dwarfed by its response to a 21%-11%-21%-11% O₂ stimulus (Figure S2C).

Having identified three *C. elegans* neuron classes that responded strongly to CO₂ and a further three that responded weakly to CO₂, we considered the possibility that all sensory neurons show some CO₂ responsiveness. Therefore, we imaged

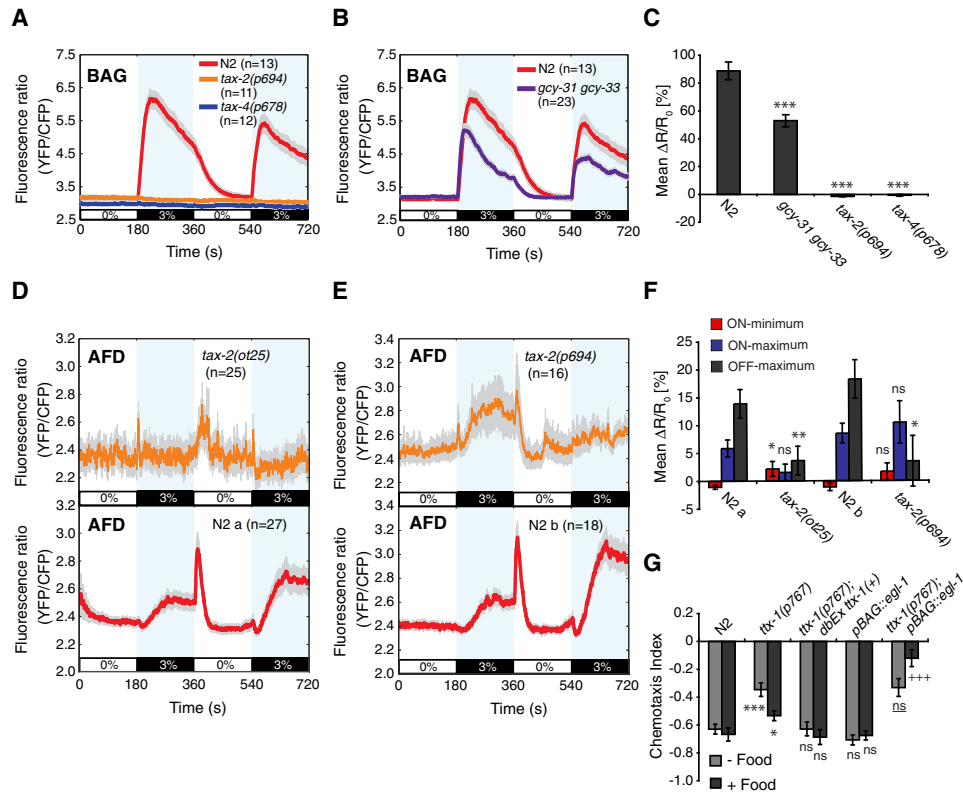


Figure 5. A cGMP Pathway Couples CO₂ to BAG and AFD Activation, and These Neurons Are Required for CO₂ Avoidance

(A) Mutations in the *tax-2* and *tax-4* cGMP-gated ion channel subunits abolish BAG responses to 3% CO₂.

(B) Mean BAG responses to 3% CO₂ in wild-type and *gcy-31(ok296) gcy-33(ok232)* double-mutant animals.

(C) Mean percent (%) $\Delta R/R_0$ values for the BAG responses in (A) and (B).

(D and E) Mean AFD response to 3% CO₂ of *tax-2(ot25)* null (D) and *tax-2(p694)* promoter deletion (E) mutants and their wild-type controls. Longer exposure times were used in imaging AFD in *tax-2(ot25)* animals due to weak expression of YC3.60.

(F) Mean percent (%) $\Delta R/R_0$ values for the AFD ON-minima, ON-maxima, and OFF-maxima of *tax-2(ot25)*, *tax-2(p694)*, and wild-type. Significance markers indicate comparisons against wild-type.

(G) AFD and BAG both contribute to CO₂ avoidance in shallow spatial gradients. *ttx-1* mutants have defects in CO₂ avoidance both on and off food. These defects are fully rescued by *ttx-1(+)* genomic DNA. Genetic ablation of BAG alone does not disrupt CO₂ avoidance, but loss of BAG when AFD is absent further disrupts CO₂ avoidance on food. Asterisks (*) and "ns" indicate significance comparisons against N2 wild-type. Plus signs (+) and "ns" indicate significance comparisons against *ttx-1(p767)* mutants.

Ca²⁺ responses to CO₂ in the ASH neurons that respond to various aversive stimuli (Hilliard et al., 2005). ASH showed no response to 3% CO₂ (Figure 4H). This suggests that AFD, BAG, and ASE are functionally specialized as CO₂ sensors.

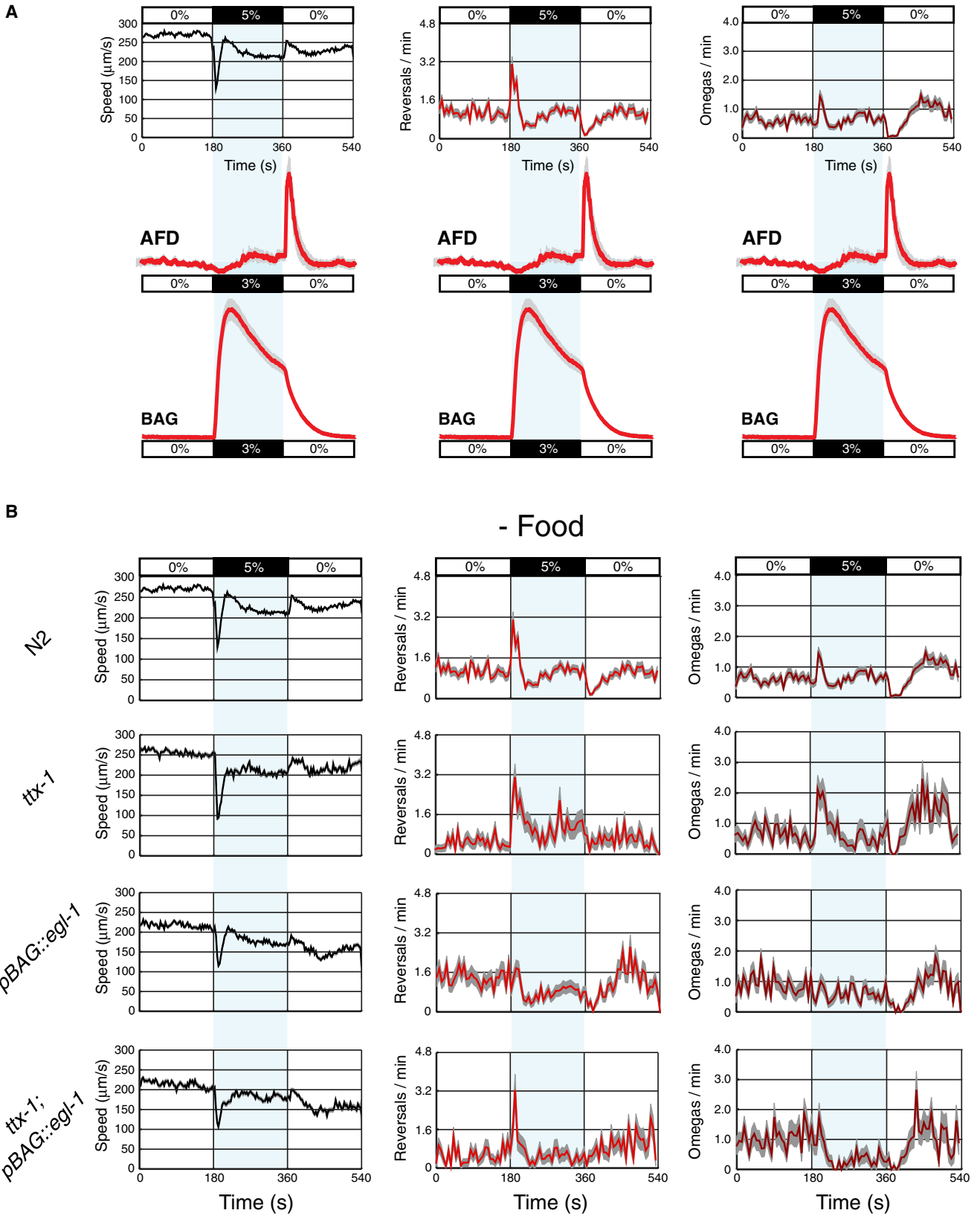
CO₂ Sensitivity in BAG and AFD Requires a cGMP-Gated Ion Channel

Our *tax-2* rescue data suggested that CO₂ sensing in BAG and AFD neurons involves cGMP signaling. To examine this further we imaged BAG responses to CO₂ in *tax-2(p694)* and *tax-4(null)* mutants. Both mutations completely abolished CO₂-evoked Ca²⁺ responses in BAG (Figures 5A and 5C). This suggests that BAG CO₂ sensory transduction is mediated by TAX-2/TAX-4 cGMP-gated channels and by extension, upstream guanylate cyclases (*gcy*).

The only *gcy* genes known to be expressed in BAG are the atypical soluble guanylate cyclases *gcy-31* and *gcy-33* (Yu et al., 1997; Zimmer et al., 2009; Ortiz et al., 2006). These

appear to be O₂ regulated (Gray et al., 2004; Boon and Marletta, 2005) because both are required for BAG O₂ responses (Zimmer et al., 2009). To examine if GCY-31, GCY-33, or both are required in CO₂ sensory transduction, we imaged BAG responses to 3% CO₂ in *gcy-31; gcy-33* double-deletion mutants. Loss of *gcy-31* and *gcy-33* reduced the CO₂-evoked BAG Ca²⁺ response (Figures 5B and 5C). This suggests that GCY-31 and/or GCY-33 forms part of the CO₂ sensory system in BAG, although other molecules are likely to be involved.

We next imaged AFD responses in *tax-2(null)* and *tax-2(p694)* animals. Expression from the *gcy-8* promoter is markedly reduced in *tax-2* and *tax-4* mutants (Satterlee et al., 2004), and YC3.60 expression was correspondingly low in AFD in *tax-2(ot25null)* animals. In contrast, expression in *tax-2(p694)* animals was similar to wild-type (data not shown). Both *tax-2* mutations significantly reduced the AFD CO₂ response, but neither completely abolished it (Figures 5D–5F). The AFD ON-minimum appeared to be absent in both *tax-2* mutants, whereas the AFD



ON-maximum was absent in *tax-2(null)* animals but enhanced in *tax-2(p694)* animals (Figures 5D–5F). Our data suggest that all three components of the AFD CO₂ response involve TAX-2 mediated cGMP pathways but that other pathways also contribute.

***C. elegans* Carbonic Anhydrases Are Expressed in Several Neurons, Including BAG**

To further investigate molecular mechanisms of CO₂ sensing, we asked whether *C. elegans* CO₂ sensors express carbonic anhydrases, hallmarks of CO₂-responsive neurons in other animals (Hu et al., 2007; Wang et al., 2002; Ridderstrale and Hanson, 1985; Coates et al., 1998). Database searches indicate that the *C. elegans* genome encodes eight predicted carbonic anhydrases. Six, *cah-1* to *cah-6*, belong to the alpha family, and two, *bca-1* and *bca-2*, to the beta family. Because many members of the beta family are mitochondrial (Syrjänen et al., 2010; Fasseas et al., 2010), we focused our studies on the alpha family. We fused upstream promoter regions of each gene to *gfp* and examined the resulting expression patterns. We found that *cah-1*, 2, 3, and 6 show strong neuronal expression in adults (Figure S3A). *cah-4* was primarily expressed in the hypodermis (excluding the seam cells) and in the excretory cell, consistent with a kidney-like function for this cell. *cah-3* and *cah-5* show expression in intestinal cells, with *cah-3* expression being especially strong. Using a *pBAG::mCherry* marker, we showed that *cah-2*, but not apparently any of the other five *cah* genes, was expressed in BAG (Figure S3B). *cah-2* was also expressed in a set of four quadrant head neurons, other unidentified head neurons, the canal neurons CANL/R, whose processes run parallel to the tracts of the excretory cell, and a pair of tail neurons (Figure S5). Previous data suggest that *cah-2* is also expressed in AFD (Colosimo et al., 2004). These data suggest that BAG and AFD neurons are specialized CO₂ sensors that coexpress carbonic anhydrases and CO₂-regulated cGMP pathways. They also raise the possibility that other *C. elegans* neurons and tissues respond to CO₂.

AFD and BAG Direct Avoidance Behavior in Spatial CO₂ Gradients

To investigate how CO₂ sensors contribute to avoidance in spatial gradients, we genetically ablated neurons. We focused on AFD and BAG neurons because the Ca²⁺ responses of ASE to CO₂ stimuli were slow, and those of AQR, PQR, and URX, weak. Specification of the AFD neurons requires the *otd/Otx* homeodomain transcription factor *ttx-1*, which is expressed only in AFD (Satterlee et al., 2001). *ttx-1* mutants show thermotactic defects equivalent to those of animals in which AFD has been removed by laser ablation (Mori and Ohshima, 1995). *ttx-1* mutants had a strong CO₂ avoidance defect off food, and a weaker defect on food (Figure 5G). Wild-type avoidance was restored to *ttx-1* mutants by a transgene containing *ttx-1*

genomic DNA (Figure 5G). These data suggest that the AFD neurons promote CO₂ avoidance in spatial CO₂ gradients.

To ablate BAG we expressed the *egl-1* programmed cell death activator from a BAG-specific *gcy-33* promoter (Conradt and Horvitz, 1998; Yu et al., 1997) (we thank M. Beverly and P. Sengupta for this line). Both BAGL and BAGR neurons were absent in greater than 90% of animals bearing this transgene (Table S1 available online). Surprisingly, the CO₂ avoidance of BAG-ablated animals was not significantly different from wild-type, both on and off food (Figure 5G). We asked if combined genetic ablation of AFD and BAG causes a synthetic CO₂ avoidance phenotype. Ablating the BAG neurons disrupted the residual CO₂ avoidance of *ttx-1(p767)* mutants on food (Figure 5G). However, in the absence of food, *ttx-1(p767); pgcy-33::egl-1* animals showed no greater defect than *ttx-1(p767)* single mutants (Figure 5G). These data show that AFD and BAG promote CO₂ avoidance in spatial gradients on food, and that AFD and at least one other neuron that is not BAG promote avoidance when food is absent. Thus, the importance of different sensory neurons for CO₂ avoidance in spatial gradients depends on context.

AFD and BAG Control Discrete Aspects of the *C. elegans* Response to CO₂

In 5%-0% CO₂ spatial gradients (Figure 1), a *C. elegans* moving at ~0.3 mm/s experiences a change of 0%-0.05% CO₂/s, depending on bearing relative to the gradient. In our Ca²⁺-imaging experiments, immobilized animals experienced much sharper temporal gradients of ~1% CO₂/s. In the wild, animals are likely to encounter a variety of CO₂ gradients. To analyze behavioral responses to sharp CO₂ gradients, we designed a square-shaped microfluidic chamber that enables CO₂ levels over freely moving animals to be switched rapidly (Movie S1 available online). We recorded responses and used custom software to extract instantaneous speed, reversal rate, and rate of omega turns, turns in which an animal's head and tail touch to form an "Ω" shape (N2, Figure 6B). In the absence of food, a rise in CO₂ from 0% to 5% elicited a brief slowing followed by a transient increase in reversals and omega turns (Figure 6B). A rapid drop in CO₂, from 5% to 0%, elicited an acceleration that coincided with suppression of reversals and omega turns.

The timing of CO₂-evoked Ca²⁺ responses in both AFD and BAG correlated with peaks in locomotory activity (Figure 6A). We investigated these correlations directly by ablating AFD and/or BAG and examining behavioral responses (Figure 6B). For statistical comparison, we chose time intervals before and after gas switches according to the occurrence of peaks in wild-type behavioral rates. In the absence of food, neither AFD nor BAG ablation abolished modulation of speed across shifts in CO₂ (Figures 6B and S4). Stronger phenotypes were observed for reversal and omega rates (Figure 6B). Unexpectedly, ablation of AFD increased reversal and omega rates following a sharp

Figure 6. AFD and BAG Control Behavioral Responses to Changes in Percent (%) CO₂

(A) AFD and BAG CO₂-evoked neuronal events correlate with CO₂-evoked behavioral events. Behavioral plots reproduced from (B). (B) Average speed, reversal, and omega rates of wild-type (N2), AFD-ablated (*ttx-1*), BAG-ablated (*pgcy-33::egl-1*), and AFD-ablated BAG-ablated (*ttx-1; pgcy-33::egl-1*) animals off food across a 0%-5%-0% CO₂ stimulus. Stimulus bar and light blue shading indicate the timing of gas switches. Gray shading indicates SEM. Speed (μm/s, black line) calculated in 3 s bins. Reversal (orange line) and omega rates (maroon line) are in event initiations per animal per minute calculated in 6 s bins. N2, n = 59 movies; *ttx-1(p767)*, n = 20 movies; *pgcy-33::egl-1*, n = 15 movies; *ttx-1; pgcy-33::egl-1*, n = 16 movies.

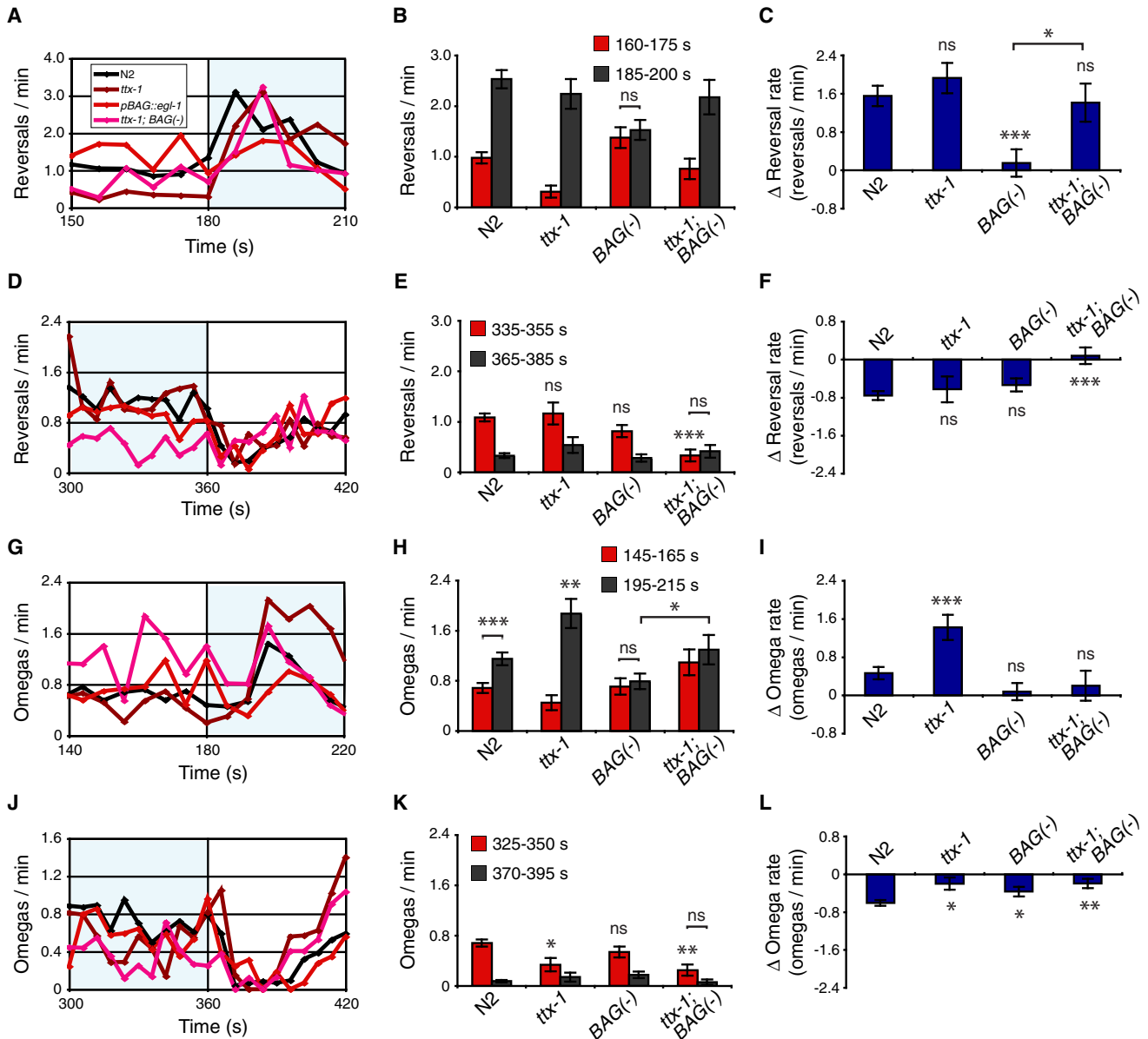


Figure 7. AFD and BAG Together Promote Turning When CO₂ Levels Rise and Inhibit Turning When CO₂ Levels Fall

(A–L) Statistical analysis of reversal and omega turns of wild-type and ablated animals during 0%-5% CO₂ increases and 5%-0% CO₂ decreases. Average behavioral traces are shown at left, time-averaged behavioral rates before and after gas switches are shown at middle, and average changes in behavioral rates are shown at right. Rates are in initiations of reversals or omega events per animal per minute. (A, D, G, and J) Average reversal and omega rates during 0%-5% CO₂ and 5%-0% CO₂ gas switches. Error bars omitted for clarity. (B, E, H, and K) Time-averaged reversal (B and E) and omega (H and K) rates before (red bars) and after (dark gray bars) an increase (B and H) or a decrease (E and K) in percent (%) CO₂. Intervals for comparison coincide with stationary points in wild-type behavioral rates. Error bars indicate SEM. (C, F, I, and L) Average change in reversal (C and F) and omega (I and L) rates across an increase (C and I) or a decrease (F and L) in percent (%) CO₂. Difference calculations based on data in (B), (E), (H), and (K), and error bars calculated from SEM values in (B), (E), (H), and (K) using error propagation formulae. Significance markers indicate comparisons against wild-type, unless otherwise indicated.

CO₂ rise (*ttx-1*, Figures 6B, 7B, 7C, 7H, and 7I) and reduced suppression of omega turns following a CO₂ fall (*ttx-1*, Figures 6B, 7K, and 7L), suggesting that AFD acts to suppress reversals and omega turns at these two time points. Ablation of BAG abolished reversal and omega responses to a rise in CO₂ (*pBAG::egl-1*, Figures 6B, 7B, 7C, 7H, and 7I) and reduced the suppression

of omega turns following a CO₂ fall (*pBAG::egl-1*, Figures 6B, 7K, and 7L), consistent with BAG excitation promoting reversals and omega turns. Coablation of AFD and BAG abolished the suppression of reversals and omega turns following a fall in CO₂ (*ttx-1; pBAG::egl-1*, Figures 7F and 7L). This effect was due to reduced reversal and omega rates under prolonged

high CO₂ (*ttx-1*; *pBAG::egl-1*, red bars, Figures 7E and 7K). These data suggest that together BAG and AFD act to suppress reversals and omega turns when CO₂ decreases.

Curiously, AFD-ablated BAG-ablated animals continued to show a transient increase in reversals following a CO₂ rise (*ttx-1*; *pBAG::egl-1*, Figures 6B, 7B, and 7C). This result suggests that there is at least one other CO₂ “ON” sensory neuron, XYZ, that promotes reversals in response to a CO₂ rise. It also suggests that after a CO₂ rise, AFD acts antagonistically to both BAG and the hypothetical XYZ neuron to inhibit reversals. We investigated whether the ASE or AQR, PQR, URX neurons could be XYZ by ablating them together with AFD and BAG. Ablating ASEL/R had no significant effect on the reversal rate of AFD-ablated BAG-ablated animals immediately following a CO₂ rise (*che-1*; *ttx-1*; *pBAG::egl-1*, Figures S5A–S5D) but did alter reversal rates under prolonged high CO₂ (Figures S5E and S5F). The ablation of AQR, PQR, URX by an integrated *pgcy-36::egl-1* transgene caused an increase in the reversal rate of AFD-ablated BAG-ablated animals in air alone (Figures S5A–S5D). These data suggest that the ASE neurons suppress reversals under prolonged high CO₂ and that the AQR, PQR, URX neurons suppress reversals in the absence of CO₂. However, even animals defective in AFD, BAG, ASE, AQR, PQR, and URX retained some CO₂ responsiveness, suggesting that *C. elegans* has additional CO₂ sensors.

The Presence of Food Modulates the Neural Circuit Controlling CO₂ Avoidance

Wild-type *C. elegans* (N2) exhibit distinct locomotory patterns in the presence and absence of food (de Bono and Bargmann 1998; Sawin et al., 2000). Animals move slowly and reverse frequently on food, whereas in its absence they move rapidly with fewer reversals. The escape mechanisms elicited by a CO₂ rise on and off food were correspondingly different (Movies S1 and S2 and Figure S6). Feeding animals still briefly slowed down when CO₂ levels rose but then switched to a high locomotory rate as high CO₂ persisted (Figure S6) (Bretscher et al., 2008). Coupled to the slowing response was a much stronger transient increase in omega turns (Figure S6). Feeding animals also persistently suppressed reversals in high CO₂. These mechanisms increased the exploratory behavior of feeding animals, presumably helping them to escape from high CO₂.

To investigate whether AFD and BAG contribute to differences between on- and off-food behavior, we ablated them. AFD ablation abolished the increased speed response to high CO₂ and resulted in inappropriately high-reversal and omega rates under high CO₂ (*ttx-1*, Figure S6). In contrast, ablating only BAG had little or no effect (*pBAG::egl-1*, Figure S6). Ablating neither AFD nor BAG alone abolished the dramatic spike in omega turns following a CO₂ rise, but ablating both neurons together nearly did (*ttx-1*; *pBAG::egl-1*, Figure S6). As for off food, loss of AFD and BAG did not eliminate CO₂ responses, suggesting that other neurons contribute to rapid CO₂-evoked behavior on food.

In summary, genetic ablation suggests that AFD and BAG account for much of the different behavioral strategies employed in CO₂ avoidance on and off food. In both contexts one or more other neurons also contribute to CO₂ avoidance.

DISCUSSION

The AFD, BAG, and ASE Sensory Neurons Exhibit Distinct CO₂ Responses

C. elegans, like mammals, monitors CO₂ using multiple neuron types. CO₂ sensors include the ASE neurons with sensory endings directly exposed to the external environment and AFD and BAG neurons whose dendrites lie within the animal. All three neuron types are primary CO₂ sensors: their CO₂ responses are unimpaired in *unc-13* mutants defective in synaptic release. Each neuron type has a unique CO₂ response. In AFD, a rise in CO₂ triggers an initial drop in intracellular Ca²⁺ levels (AFD ON-minimum), then a rise above baseline (AFD ON-maximum), and when CO₂ is removed, a spike (AFD OFF-maximum). This complexity may reflect multiple CO₂-transduction mechanisms. In contrast, BAG and ASE neurons are activated by a rise, but not a fall, in CO₂. In BAG, Ca²⁺ peaks within 60 s of a rise in CO₂, then decays to a plateau that persists as long as CO₂ remains high; Ca²⁺ drops back to baseline upon CO₂ removal. ASE responds slowly to CO₂ exposure: Ca²⁺ takes 2 min to peak but remains elevated while CO₂ is high. The tonic activity of BAG and ASE neurons in high CO₂ may allow *C. elegans* to modify responses to other cues, perhaps by affecting sensory pathways or inter-neuron networks.

AFD, BAG, and ASE also sense other stimuli. AFD senses temperature (Kimura et al., 2004), BAG senses ambient O₂ (Zimmer et al., 2009), and ASE senses salt (Suzuki et al., 2008). This may enable sensory integration within sensory neurons. For each of the three neurons, CO₂ and non-CO₂ stimuli evoke distinct Ca²⁺ responses. When temperature rises above the cultivation level, AFD responds with a monophasic Ca²⁺ spike that lasts a few seconds (Kimura et al., 2004; Clark et al., 2007). The dissimilar CO₂ and temperature responses suggest that the two stimuli are sensed differently. Supporting this, AFD responds to CO₂ below the cultivation temperature. The Ca²⁺ responses of BAG to high CO₂ and low O₂ are more similar in shape (Figure 3) (Zimmer et al., 2009). In contrast, the responses of ASE to CO₂ and NaCl differ markedly (Figure 4) (Suzuki et al., 2008). First, unlike CO₂, NaCl evokes an asymmetric response in ASEL and ASER: a rise in NaCl triggers a Ca²⁺ spike in ASEL but a drop in Ca²⁺ in ASER. Second, ASEL/R Ca²⁺ responses to NaCl adapt rapidly, whereas sustained CO₂ stimulation leads to sustained high Ca²⁺ in ASE (Figure 4F). Third, whereas ASE responses to CO₂ are slow, taking around 2 min for Ca²⁺ to peak, responses to NaCl peak within 30 s of stimulus exposure. The slowness of ASE CO₂ responses could reflect rate-limiting hydration of environmental CO₂.

cGMP Signaling Mediates CO₂ Responses

CO₂ sensing in AFD, BAG, and ASE involves cGMP signaling. Mutating the cGMP-gated channel subunit *tax-2* partially abolishes the AFD Ca²⁺ response to CO₂ and completely abolishes CO₂-evoked activity in BAG (Figure 5). CO₂-evoked Ca²⁺ responses in ASE likely also depend on cGMP-gated channels because expression of *tax-2* cDNA in ASE in *tax-2* mutants partially restores CO₂ avoidance (Figure 1). In mouse olfactory epithelia, CO₂ sensing requires the transmembrane guanylate cyclase GC-D, which is activated by HCO₃⁻ (Hu et al., 2007;

Sun et al., 2009). The hallmarks that make GC-D HCO₃⁻ regulated are unknown, but the *C. elegans* genome encodes 27 transmembrane guanylate cyclase (*gcy*), a subset of which could be similarly regulated (Yu et al., 1997; Ortiz et al., 2006). The AFD neurons express *gcy-8*, *gcy-18*, *gcy-23*, and *gcy-29*. *gcy-8 gcy-18 gcy-23* triple mutants have a thermotaxis defect similar to that of the AFD specification mutant *ttx-1* (Inada et al., 2006), but have no defect in CO₂ avoidance in a 5%-0% CO₂ gradient (data not shown). ASE neurons express 11 transmembrane guanylate cyclases, nine of which are expressed asymmetrically either in ASEL or ASER (Ortiz et al., 2006).

Transmembrane guanylate cyclase expression has not been reported in BAG. However, BAG expresses the atypical soluble guanylate cyclases GCY-31 and GCY-33 (Yu et al., 1997). Simultaneously disrupting *gcy-31* and *gcy-33* reduced the CO₂-evoked Ca²⁺ response amplitudes in BAG, suggesting that GCY-31 and/or GCY-33 contribute to CO₂ sensing. GCY-31 and GCY-33 are thought to function as heterodimers that have an O₂-binding heme cofactor (Boon and Marletta, 2005) and are required for BAG O₂-evoked Ca²⁺ responses when O₂ drops below 10% (Zimmer et al., 2009). An intriguing possibility is that the GCY-31/GCY-33 heterodimer is inhibited by O₂ and activated by CO₂, making it a sensory integrator of CO₂ and O₂ signals in BAG (Figure 8A); however, we cannot rule out the possibility of a linked mutation disrupting BAG responses.

AFD, BAG, and ASE are unlikely to be the only CO₂-responsive neurons in *C. elegans*. The AQR, PQR, and URX O₂-sensing neurons showed sporadic responses to CO₂ (Figure S2), and selective expression of *tax-2* cDNA in these neurons partially restored CO₂ avoidance to *tax-2(p694)* mutants, suggesting that they are CO₂ sensitive. Moreover, more than ten *C. elegans* neurons express carbonic anhydrases, some of which may be unidentified CO₂ sensors.

The Contribution of Different Sensors to CO₂ Avoidance Varies with Stimulus Dynamics and Context

Why does *C. elegans* have multiple CO₂ sensors? One reason is that sensors are deployed differently according to the dynamics of the CO₂ stimulus. For example, when food is absent, BAG mediates responses to sharp CO₂ gradients but is less important for navigating shallow gradients (compare Figures 5G and 6B). A second reason is that context modifies the behavioral changes needed to escape CO₂. For example, when food is present, *C. elegans* move slowly and reverse frequently. To efficiently escape high CO₂ in a food-containing environment, *C. elegans* increase speed and suppress reversals relative to the “on food” ground state. By contrast when food is absent, animals are already moving quickly and reversing less frequently. Correspondingly, the importance of BAG for CO₂ avoidance depends on both stimulus shape and food context. Whereas BAG-ablated animals respond poorly to rapid CO₂ changes when food is absent, they respond like wild-type animals when food is present (*pBAG::egl-1*, Figures 6 and S6). Conversely, in shallow gradients BAG acts redundantly with AFD to promote CO₂ avoidance when food is present but is not important when food is absent, even when AFD is ablated (Figure 5G).

How do the Ca²⁺ responses of CO₂ sensory neurons encode behavior? CO₂-evoked neuronal events in AFD and BAG corre-

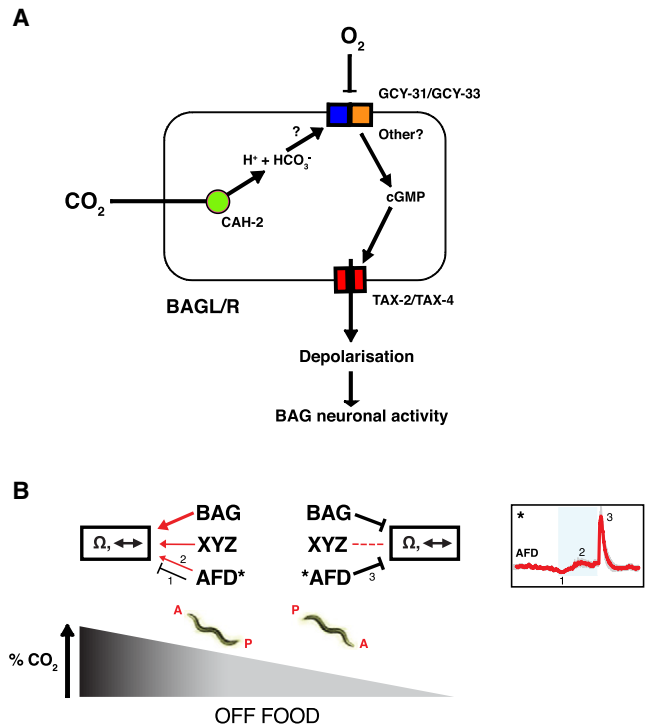


Figure 8. Models of CO₂ Sensory Neuron Function

(A) Model of CO₂ and O₂-evoked excitability in the BAG neurons. As in mouse CO₂ olfactory neurons, a carbonic anhydrase CAH-2 catalyzes hydration of CO₂ in BAG. HCO₃⁻ ions or H⁺ protons may activate the GCY-31/GCY-33 heterodimer as well as another guanylate cyclase. Elevated cGMP levels open the TAX-2/TAX-4 channel causing Ca²⁺ influx and BAG depolarization.

(B) AFD, BAG, and the postulated CO₂-ON sensory neuron XYZ ensure turning probability increases when the CO₂ gradient is positive and decreases when negative. As an animal moves up a CO₂ gradient, increasing CO₂ activates BAG and XYZ, which activate turning. AFD initially inhibits turning (ON-minimum, 1), but as Ca²⁺ levels rise (ON-maximum, 2), AFD promotes turning. As an animal moves down a CO₂ gradient, a decrease in CO₂ causes deactivation of BAG and the AFD OFF-response (3), which suppress turning. Activation is represented by red arrows, and inhibition, by black “T” symbols. The worm at left is heading up the gradient, and the worm at right, down the gradient. A, anterior; P, posterior. “Ω” represents omega turns and the double-headed arrow, reversals.

late with peaks and troughs in locomotory rates (Figure 6A). To investigate these relationships, we ablated CO₂ sensors. One caveat of neuronal ablation is that it can only remove a neuron in its entirety, and not individual components of its responses. Ablation of AFD and BAG neurons one at a time and together suggests that: (1) BAG activation and the AFD ON-minimum act antagonistically, promoting and suppressing reversal and omega rates, respectively (Figures 7C and 7I); (2) BAG plateau activity and the AFD ON-maximum both act to promote reversal and omega rates during maintained high CO₂ (*ttx-1*; *BAG*⁻), Figures 7E and 7K); and (3) decay of BAG activity and the AFD OFF-maximum act together to suppress reversals and omega turns following CO₂ removal (*ttx-1*; *BAG*⁻), Figures 7F and 7L). Together our data suggest that when an animal is migrating up a CO₂ gradient, BAG and AFD trigger turning, whereas when

an animal is migrating down a CO₂ gradient, AFD and BAG suppress turning (Figure 8B). Therefore, it appears that the three different components of the AFD CO₂ response may differentially regulate behavior (1, 2, 3, AFD, Figure 8B). Because AFD(-) BAG (-) animals still respond to CO₂, we also infer the existence of an additional sensory neuron, XYZ, that is neither ASE nor AQR, PQR, URX, that promotes turning when CO₂ rises (Figure 8B).

CO₂ Avoidance Behavior in *C. elegans* Appears to Be a Homeostatic Mechanism

Elevated tissue CO₂ is toxic (Richerson, 2004). In *C. elegans*, CO₂ levels exceeding 9% disrupt body muscle organization and general development and reduce fertility (Sharabi et al., 2009). The CO₂ responses of AFD, BAG, and ASE neurons do not habituate upon multiple exposures to CO₂ (Figures 2 and 3; data not shown). *C. elegans* CO₂ avoidance in spatial gradients is also nonhabituating over a similar period (data not shown). By contrast, *C. elegans* attraction to benzaldehyde (L'Etoile et al., 2002), response to noxious Cu²⁺ ion stimuli (Hilliard et al., 2005), and response to nose touch (Kindt et al., 2007) all habituate. Moreover, BAG and ASE neurons show tonic signaling while CO₂ levels are high, at least over 20 min. We speculate that *C. elegans* CO₂ avoidance habituates slowly and performs a homeostatic function by preventing CO₂ poisoning of body tissues. *C. elegans* CO₂ avoidance provides an opportunity for detailed examination of a CO₂ homeostatic system with comparative ease relative to the systems of more complex animals.

EXPERIMENTAL PROCEDURES

Strains

Strains were grown at 22°C under standard conditions (Brenner, 1974). Mutant combinations were made by following visible phenotypes or using PCR to confirm genotype. A full list of strains can be found in Supplemental Experimental Procedures.

Behavioral Assays

Spatial CO₂ gradient assays were as described (Bretscher et al., 2008). Briefly, polydimethylsiloxane (PDMS) chambers connected to gas syringe pumps were placed over adult worms on a 9 cm agar plate. After 10 min the distribution of worms was used to calculate a chemotaxis index (Figure 1). Chemotaxis bar graphs represent the average of nine independent assays performed over 3 days.

For temporal gradient assays a square 11 × 11 × 0.2 mm PDMS chamber was placed over adult worms on 6 cm agar plates. For off-food assays, ~40 animals were picked after washing in M9 Buffer to remove adhering *E. coli*. For on-food assays, a 2-day-old 20 μl *E. coli* lawn was used. Worms were allowed to crawl on food for 1 hr. After placing the chamber, animals were left for 4 min before exposure to a 0%-5%-0% CO₂ stimulus. Behavior was captured using a Grasshopper CCD camera (Point Grey Research). A TTL-output from a frame counter (custom built) controlled opening and closing of Teflon™ pinch valves (Automate Scientific) at defined time points, controlling the switching of gases. Worms were tracked using DIAS Software (Solltech), and worm object paths were created. The centroid X and Y coordinates, maximum length, mean width, perimeter, and roundness were extracted for each worm object across frames. From these parameters, speed, omega initiation rate, and reversal initiation rate were calculated using a custom-written program in MATLAB (The MathWorks). Omega turns were detected by circular object topologies. This method gave 90.9% success using the stringent criterion that worm head touches worm tail. Reversal events were defined as forward movement (F), followed by backward movement (B), followed by return to forward move-

ment (F). Using the criterion of an F-B-F event and optimized parameters minimum allowable reversal angle (150°), maximum reversal duration (7.5 s), and minimum reversal distance (0.3 mm, life size), reversal detection success rate ran at 81.25%. Detection parameters were optimized by minimizing the sum of the squared differences between detection outputs of computer and a human observer for Movie S1. Behavior occurring during merger of worm objects was discarded. Temporal gradient assay data represent the average of 16 or more movies for off food and nine or more for on food.

In all experiments, percent (%) CO₂ was balanced by percent (%) N₂ while 21% O₂ was maintained. In rescue experiments, transgenic animals were pre-selected by following coinjection markers. In all figures, statistical significance was determined using the two-tailed Student's t test.

Calcium Imaging

Ca²⁺ imaging was on an inverted microscope (Axiovert; Zeiss), using a 40× C-Apochromat lens and MetaMorph acquisition software (Molecular Devices). Agarose pads were made in M9 Buffer (pH 6.8) and 1 mM CaCl₂, mimicking an NGM substrate. Worms expressing the Ca²⁺ sensor YC3.60 showed wild-type avoidance in 5%-0% CO₂ gradients (Figure S1). Worms were glued to pads using Nexaband glue (WPI Inc.) and placed under the stem of the Y-chamber microfluidic device. Photobleaching was minimized using a 2.0 optical density filter and a shutter to limit exposure time to 100 ms per frame. An excitation filter (Chroma) restricted illumination to the cyan channel. A beam splitter (Optical Insights) was used to separate the cyan and yellow emission light. The ratio of the background-subtracted fluorescence in the YFP and CFP channels was calculated with Jmalyze (Kerr and Schafer, 2006). Fluorescence ratio (YFP/CFP) plots were made in MATLAB. Movies were captured at 2 fps. Average Ca²⁺ traces were compiled from at least six recordings made on 2 or more days.

SUPPLEMENTAL INFORMATION

Supplemental Information includes Supplemental Experimental Procedures, six figures, one table, and two movies and can be found with this article online at doi:10.1016/j.neuron.2011.02.023.

ACKNOWLEDGMENTS

We thank the Caenorhabditis Genetics Centre, the *C. elegans* Knockout Consortium, Piali Sengupta, Bill Schafer, Ikue Mori, and Oliver Hobert for strains; the Dana-Farber Cancer Institute and Source Bioscience for reagents; Robyn Branicky for comments on the manuscript; and all the de Bono and Schafer lab members for insight, help, and advice. K.E.B. was funded by the Swiss National Science Foundation, P.L. was funded by EMBO, and otherwise research was funded by either the Medical Research Council, UK, or private funds.

Accepted: December 23, 2010

Published: March 23, 2011

REFERENCES

- Bargmann, C.I., and Horvitz, H.R. (1991). Chemosensory neurons with overlapping functions direct chemotaxis to multiple chemicals in *C. elegans*. *Neuron* 7, 729–742.
- Boon, E.M., and Marletta, M.A. (2005). Ligand discrimination in soluble guanylate cyclase and the H-NOX family of heme sensor proteins. *Curr. Opin. Chem. Biol.* 9, 441–446.
- Brenner, S. (1974). The genetics of *Caenorhabditis elegans*. *Genetics* 77, 71–94.
- Bretscher, A.J., Busch, K.E., and de Bono, M. (2008). A carbon dioxide avoidance behavior is integrated with responses to ambient oxygen and food in *Caenorhabditis elegans*. *Proc. Natl. Acad. Sci. USA* 105, 8044–8049.
- Buchanan, G.F., and Richerson, G.B. (2010). Central serotonin neurons are required for arousal to CO₂. *Proc. Natl. Acad. Sci. USA* 107, 16354–16359.

- Buckler, K.J., Williams, B.A., and Honore, E. (2000). An oxygen-, acid- and anaesthetic-sensitive TASK-like background potassium channel in rat arterial chemoreceptor cells. *J. Physiol.* 525, 135–142.
- Bustami, H.P., Harrison, J.F., and Hustert, R. (2002). Evidence for oxygen and carbon dioxide receptors in insect CNS influencing ventilation. *Comp. Biochem. Physiol. A Mol. Integr. Physiol.* 133, 595–604.
- Cammer, W.B., and Brion, L.P. (2000). Carbonic anhydrase in the nervous system. *EXS* 90, 475–489.
- Chandrashekar, J., Yarmolinsky, D., von Buchholtz, L., Oka, Y., Sly, W., Ryba, N.J., and Zuker, C.S. (2009). The taste of carbonation. *Science* 326, 443–445.
- Clark, D.A., Biron, D., Sengupta, P., and Samuel, A.D. (2006). The AFD sensory neurons encode multiple functions underlying thermotactic behavior in *Caenorhabditis elegans*. *J. Neurosci.* 26, 7444–7451.
- Clark, D.A., Gabel, C.V., Gabel, H., and Samuel, A.D. (2007). Temporal activity patterns in thermosensory neurons of freely moving *Caenorhabditis elegans* encode spatial thermal gradients. *J. Neurosci.* 27, 6083–6090.
- Coates, E.L., Wells, C.M., and Smith, R.P. (1998). Identification of carbonic anhydrase activity in bullfrog olfactory receptor neurons: histochemical localization and role in CO₂ chemoreception. *J. Comp. Physiol. A* 182, 163–174.
- Coates, J.C., and de Bono, M. (2002). Antagonistic pathways in neurons exposed to body fluid regulate social feeding in *Caenorhabditis elegans*. *Nature* 419, 925–929.
- Coburn, C.M., and Bargmann, C.I. (1996). A putative cyclic nucleotide-gated channel is required for sensory development and function in *C. elegans*. *Neuron* 17, 695–706.
- Colosimo, M.E., Brown, A., Mukhopadhyay, S., Gabel, C., Lanjuin, A.E., Samuel, A.D., and Sengupta, P. (2004). Identification of thermosensory and olfactory neuron-specific genes via expression profiling of single neuron types. *Curr. Biol.* 14, 2245–2251.
- Conradt, B., and Horvitz, H.R. (1998). The *C. elegans* protein EGL-1 is required for programmed cell death and interacts with the Bcl-2-like protein CED-9. *Cell* 93, 519–529.
- de Bono, M., and Bargmann, C.I. (1998). Natural variation in a neuropeptide Y receptor homolog modifies social behavior and food response in *C. elegans*. *Cell* 94, 679–689.
- Dusenbery, D.B., Sheridan, R.E., and Russell, R.L. (1975). Chemotaxis-defective mutants of the nematode *Caenorhabditis elegans*. *Genetics* 80, 297–309.
- Fasseas, M.K., Tsikou, D., Flemetakis, E., and Katinakis, P. (2010). Molecular and biochemical analysis of the beta class carbonic anhydrases in *Caenorhabditis elegans*. *Mol. Biol. Rep.* 37, 2941–2950.
- Faucher, C., Forstreuter, M., Hilker, M., and de Bruyne, M. (2006). Behavioral responses of *Drosophila* to biogenic levels of carbon dioxide depend on life-stage, sex and olfactory context. *J. Exp. Biol.* 209, 2739–2748.
- Feldman, J.L., Mitchell, G.S., and Nattie, E.E. (2003). Breathing: rhythmicity, plasticity, chemosensitivity. *Annu. Rev. Neurosci.* 26, 239–266.
- Fischler, W., Kong, P., Marella, S., and Scott, K. (2007). The detection of carbonation by the *Drosophila* gustatory system. *Nature* 448, 1054–1057.
- Gray, J.M., Karow, D.S., Lu, H., Chang, A.J., Chang, J.S., Ellis, R.E., Marletta, M.A., and Bargmann, C.I. (2004). Oxygen sensation and social feeding mediated by a *C. elegans* guanylate cyclase homologue. *Nature* 430, 317–322.
- Hallem, E.A., and Sternberg, P.W. (2008). Acute carbon dioxide avoidance in *Caenorhabditis elegans*. *Proc. Natl. Acad. Sci. USA* 105, 8038–8043.
- Hedgecock, E.M., and Russell, R.L. (1975). Normal and mutant thermotaxis in the nematode *Caenorhabditis elegans*. *Proc. Natl. Acad. Sci. USA* 72, 4061–4065.
- Hetz, S.K., and Bradley, T.J. (2005). Insects breathe discontinuously to avoid oxygen toxicity. *Nature* 433, 516–519.
- Hilliard, M.A., Apicella, A.J., Kerr, R., Suzuki, H., Bazzicalupo, P., and Schafer, W.R. (2005). In vivo imaging of *C. elegans* ASH neurons: cellular response and adaptation to chemical repellents. *EMBO J.* 24, 63–72.
- Hobert, O., Johnston, R.J.J., and Chang, S. (2002). Left-right asymmetry in the nervous system: the *Caenorhabditis elegans* model. *Nat. Rev. Neurosci.* 3, 629–640.
- Hu, J., Zhong, C., Ding, C., Chi, Q., Walz, A., Mombaerts, P., Matsunami, H., and Luo, M. (2007). Detection of near-atmospheric concentrations of CO₂ by an olfactory subsystem in the mouse. *Science* 317, 953–957.
- Inada, H., Ito, H., Satterlee, J., Sengupta, P., Matsumoto, K., and Mori, I. (2006). Identification of guanylyl cyclases that function in thermosensory neurons of *Caenorhabditis elegans*. *Genetics* 172, 2239–2252.
- Jiang, C., Rojas, A., Wang, R., and Wang, X. (2005). CO₂ central chemosensitivity: why are there so many sensing molecules? *Respir. Physiol. Neurobiol.* 145, 115–126.
- Jones, W.D., Cayirioglu, P., Kadow, I.G., and Vosshall, L.B. (2007). Two chemosensory receptors together mediate carbon dioxide detection in *Drosophila*. *Nature* 445, 86–90.
- Kerr, R.A., and Schafer, W.R. (2006). Intracellular Ca²⁺ imaging in *C. elegans*. *Methods Mol. Biol.* 357, 253–264.
- Kimura, K.D., Miyawaki, A., Matsumoto, K., and Mori, I. (2004). The *C. elegans* thermosensory neuron AFD responds to warming. *Curr. Biol.* 14, 1291–1295.
- Kindt, K.S., Quast, K.B., Giles, A.C., De, S., Hendrey, D., Nicastro, I., Rankin, C.H., and Schafer, W.R. (2007). Dopamine mediates context-dependent modulation of sensory plasticity in *C. elegans*. *Neuron* 55, 662–676.
- Komatsu, H., Mori, I., Rhee, J.S., Akaike, N., and Ohshima, Y. (1996). Mutations in a cyclic nucleotide-gated channel lead to abnormal thermosensation and chemosensation in *C. elegans*. *Neuron* 17, 707–718.
- Kwon, J.Y., Dahanukar, A., Weiss, L.A., and Carlson, J.R. (2007). The molecular basis of CO₂ reception in *Drosophila*. *Proc. Natl. Acad. Sci. USA* 104, 3574–3578.
- Lahiri, S., and Forster, R.E., 2nd. (2003). CO₂/H⁺ sensing: peripheral and central chemoreception. *Int. J. Biochem. Cell Biol.* 35, 1413–1435.
- Lehmann, F.O., and Heymann, N. (2005). Unconventional mechanisms control cyclic respiratory gas release in flying *Drosophila*. *J. Exp. Biol.* 208, 3645–3654.
- L'Etoile, N.D., Coburn, C.M., Eastham, J., Kistler, A., Gallegos, G., and Bargmann, C.I. (2002). The cyclic GMP-dependent protein kinase EGL-4 regulates olfactory adaptation in *C. elegans*. *Neuron* 36, 1079–1089.
- Mori, I., and Ohshima, Y. (1995). Neural regulation of thermotaxis in *Caenorhabditis elegans*. *Nature* 376, 344–348.
- Ortiz, C.O., Etchberger, J.F., Posy, S.L., Frokjaer-Jensen, C., Lockery, S., Honig, B., and Hobert, O. (2006). Searching for neuronal left/right asymmetry: genomewide analysis of nematode receptor-type guanylyl cyclases. *Genetics* 173, 131–149.
- Ortiz, C.O., Faumont, S., Takayama, J., Ahmed, H.K., Goldsmith, A.D., Pocock, R., McCormick, K.E., Kunimoto, H., Iino, Y., Lockery, S., and Hobert, O. (2009). Lateralized gustatory behavior of *C. elegans* is controlled by specific receptor-type guanylyl cyclases. *Curr. Biol.* 19, 996–1004.
- Persson, A., Gross, E., Laurent, P., Busch, K.E., Bretes, H., and de Bono, M. (2009). Natural variation in a neural globin tunes oxygen sensing in wild *Caenorhabditis elegans*. *Nature* 458, 1030–1033.
- Richerson, G.B. (2004). Serotonergic neurons as carbon dioxide sensors that maintain pH homeostasis. *Nat. Rev. Neurosci.* 5, 449–461.
- Richerson, G.B., Wang, W., Hodges, M.R., Dohle, C.I., and Diez-Sampedro, A. (2005). Homing in on the specific phenotype(s) of central respiratory chemoreceptors. *Exp. Physiol.* 90, 259–266.
- Richmond, J.E., Davis, W.S., and Jorgensen, E.M. (1999). UNC-13 is required for synaptic vesicle fusion in *C. elegans*. *Nat. Neurosci.* 2, 959–964.
- Ridderstrale, Y., and Hanson, M. (1985). Histochemical study of the distribution of carbonic anhydrase in the cat brain. *Acta Physiol. Scand.* 124, 557–564.
- Satterlee, J.S., Ryu, W.S., and Sengupta, P. (2004). The CMK-1 CaMK and the TAX-4 cyclic nucleotide-gated channel regulate thermosensory neuron gene expression and function in *C. elegans*. *Curr. Biol.* 14, 62–68.

- Satterlee, J.S., Sasakura, H., Kuhara, A., Berkeley, M., Mori, I., and Sengupta, P. (2001). Specification of thermosensory neuron fate in *C. elegans* requires *ttx-1*, a homolog of *otd/Otx*. *Neuron* 31, 943–956.
- Sawin, E.R., Ranganathan, R., and Horvitz, H.R. (2000). *C. elegans* locomotory rate is modulated by the environment through a dopaminergic pathway and by experience through a serotonergic pathway. *Neuron* 26, 619–631.
- Sharabi, K., Hurwitz, A., Simon, A.J., Beitel, G.J., Morimoto, R.I., Rechavi, G., Sznajder, J.I., and Gruenbaum, Y. (2009). Elevated CO₂ levels affect development, motility, and fertility and extend life span in *Caenorhabditis elegans*. *Proc. Natl. Acad. Sci. USA* 106, 4024–4029.
- Speese, S., Petrie, M., Schuske, K., Ailion, M., Ann, K., Iwasaki, K., Jorgensen, E.M., and Martin, T.F. (2007). UNC-31 (CAPS) is required for dense-core vesicle but not synaptic vesicle exocytosis in *Caenorhabditis elegans*. *J. Neurosci.* 27, 6150–6162.
- Suh, G.S., Wong, A.M., Hergarden, A.C., Wang, J.W., Simon, A.F., Benzer, S., Axel, R., and Anderson, D.J. (2004). A single population of olfactory sensory neurons mediates an innate avoidance behavior in *Drosophila*. *Nature* 431, 854–859.
- Suh, G.S., Ben-Tabou de Leon, S., Tanimoto, H., Fiala, A., Benzer, S., and Anderson, D.J. (2007). Light activation of an innate olfactory avoidance response in *Drosophila*. *Curr. Biol.* 17, 905–908.
- Sun, L., Wang, H., Hu, J., Han, J., Matsunami, H., and Luo, M. (2009). Guanylyl cyclase-D in the olfactory CO₂ neurons is activated by bicarbonate. *Proc. Natl. Acad. Sci. USA* 106, 2041–2046.
- Suzuki, H., Thiele, T.R., Faumont, S., Ezcurra, M., Lockery, S.R., and Schafer, W.R. (2008). Functional asymmetry in *Caenorhabditis elegans* taste neurons and its computational role in chemotaxis. *Nature* 454, 114–117.
- Syrjänen, L., Tolvanen, M., Hilvo, M., Olatubosun, A., Innocenti, A., Scozzafava, A., Leppiniemi, J., Niederhauser, B., Hytonen, V.P., Gorr, T.A., et al. (2010). Characterization of the first beta-class carbonic anhydrase from an arthropod (*Drosophila melanogaster*) and phylogenetic analysis of beta-class carbonic anhydrases in invertebrates. *BMC Biochem.* 11, 28.
- Turner, S.L., and Ray, A. (2009). Modification of CO₂ avoidance behavior in *Drosophila* by inhibitory odorants. *Nature* 461, 277–281.
- Vosshall, L.B., and Stocker, R.F. (2007). Molecular architecture of smell and taste in *Drosophila*. *Annu. Rev. Neurosci.* 30, 505–533.
- Wang, W., Bradley, S.R., and Richerson, G.B. (2002). Quantification of the response of rat medullary raphe neurones to independent changes in pH_o and pCO₂. *J. Physiol.* 540, 951–970.
- Ward, S., Thomson, N., White, J.G., and Brenner, S. (1975). Electron microscopical reconstruction of the anterior sensory anatomy of the nematode *Caenorhabditis elegans*. *J. Comp. Neurol.* 160, 313–337.
- White, J.G., Southgate, E., Thomson, J.N., and Brenner, S. (1986). The structure of the nervous system of the nematode *Caenorhabditis elegans*. *Philos. Trans. R. Soc. Lond. B Biol. Sci.* 314, 1–340.
- Williams, R.H., Jensen, L.T., Verkhatsky, A., Fugger, L., and Burdakov, D. (2007). Control of hypothalamic orexin neurons by acid and CO₂. *Proc. Natl. Acad. Sci. USA* 104, 10685–10690.
- Young, J.M., Waters, H., Dong, C., Fulle, H.J., and Liman, E.R. (2007). Degeneration of the olfactory guanylyl cyclase D gene during primate evolution. *PLoS ONE* 2, e884.
- Yu, S., Avery, L., Baude, E., and Garbers, D.L. (1997). Guanylyl cyclase expression in specific sensory neurons: a new family of chemosensory receptors. *Proc. Natl. Acad. Sci. USA* 94, 3384–3387.
- Ziemann, A.E., Allen, J.E., Dahdaleh, N.S., Drebot, I.I., Coryell, M.W., Wunsch, A.M., Lynch, C.M., Faraci, F.M., Howard, M.A.R., Welsh, M.J., and Wemmie, J.A. (2009). The amygdala is a chemosensor that detects carbon dioxide and acidosis to elicit fear behavior. *Cell* 139, 1012–1021.
- Zimmer, M., Gray, J.M., Pokala, N., Chang, A.J., Karow, D.S., Marletta, M.A., Hudson, M.L., Morton, D.B., Chronis, N., and Bargmann, C.I. (2009). Neurons detect increases and decreases in oxygen levels using distinct guanylate cyclases. *Neuron* 61, 865–879.